A physics-based approach to modeling real-fuel combustion chemistry – V. NO$_x$ formation from a typical Jet A

Chiara Saggese [a,1], Kevin Wan [a], Rui Xu [a], Yujie Tao [a,2], Craig T. Bowman [a], Ji-Woong Park [b], Tianfeng Lu [b], Hai Wang [a,*]

[a] Department of Mechanical Engineering, Stanford University, Stanford, CA 94305-3032, USA
[b] Department of Mechanical Engineering, University of Connecticut, Storrs, CT 06269-3139, USA

ABSTRACT

Real transportation fuels are complex mixtures of a variety of hydrocarbon components. Predicting NO$_x$ formation in practical combustors burning real fuels is usually made with the assumption that the NO$_x$ submodels developed and tested for small hydrocarbon combustion are applicable to mixtures of large hydrocarbons as found in real fuels. Additionally, NO$_x$ data are scarce for flames of real fuels. The aims of the current study are (i) to provide reliable NO$_x$ data in flames of a typical jet fuel, and (ii) to test our capability to predict these data by combining a recently proposed HyChem reaction model of jet A combustion (Xu et al., 2018) with the NO$_x$ submodel of Glarborg (2018). Specifically, NO$_x$ concentrations were measured in stretch-stabilized premixed flames of methane and Jet A (POSF10325) from fuel lean to rich conditions and of ethylene at a fuel-rich equivalence ratio. This range of stoichiometries allows both thermal NO and prompt NO pathways to be tested. The results show reasonably good agreement between the experimental data and model predictions for all flames tested, although the model appears to underpredict NO$_x$ concentrations in the Jet A flames under fuel rich conditions. Sensitivity analyses were conducted to illustrate the influence of the reaction pathways and flame boundary conditions on NO$_x$ predictions. The analyses also suggest that additional prompt NO reaction pathways may play a role in flames of large hydrocarbons.

© 2019 The Combustion Institute. Published by Elsevier Inc. All rights reserved.

Introduction

We recently proposed the Hybrid Chemistry (HyChem) approach to modeling the high-temperature combustion chemistry of liquid, distillate fuels [1–3]. As a physics-based approach, HyChem seeks to establish the direct cause and effect governing the combustion chemistry of real, liquid fuels that are multicomponent in nature. The approach assumes that during high-temperature combustion fuel pyrolysis or oxidative pyrolysis precedes the oxidation of the pyrolysis products and that the combustion properties of distillate fuels are controlled primarily by the major pyrolysis products. The compositional variations of a fuel are often washed out due to the principle of large component number [1, 4]. Since the key pyrolysis products are substantially less diverse in number and

complexity than the initial fuel, they can be closely followed in shock tubes and flow reactor experiments. Hence, HyChem uses lumped reaction steps and associated kinetics for fuel pyrolysis, which may be probed directly by experiments. By combining the lumped reaction steps with a suitable foundational fuel chemistry model, we have demonstrated that HyChem models are viable for making useful predictions of global combustion properties, including laminar flame speed, flame extinction, and homogeneous ignition for a wide range of aviation and rocket fuels [1–3, 5]. The resulting reaction models are compact in size and can be reduced to 30 to 40 species without drastically impacting the predictive capabilities [1–3, 5]. The approach enables computational fluid dynamics simulations of turbulent combustion behaviors of real fuels in practical combustors or under practical combustor conditions (see, e.g., [6–14]).

The purpose of the present work is to extend the HyChem model to predicting nitrogen oxide (NO$_x$) formation. For this purpose, we choose a conventional Jet A (designated as A2 in the recent National Jet Fuel Combustion Program [15]) as the test fuel. A significant amount of work about NO$_x$ formation mechanisms [16–18] shows that in absence of fuel NO$_x$, the thermal NO
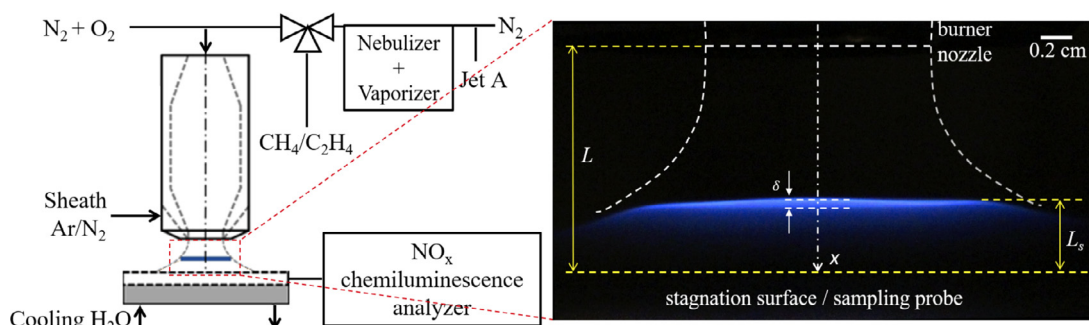
Fig. 1. Schematic experimental setup and a typical image of Jet A flame.

[19] and prompt NO [20] are the dominant paths to NO production in fuel combustion. Additional reaction paths includes the production of N_2O from $O + N_2 (+M) = N_2O (+M)$ [21] and of NNH from $H + N_2 (+M) = NNH (+M)$ [22], followed by oxidation of the nitrogen intermediate to NO. These NO paths are primarily related to main-flame chemistry, and as such they are largely decoupled from the fuel pyrolysis process that precedes the main flame. We therefore expect that when combined with an appropriate NO_x submodel, the HyChem model should predict NO_x production in Jet A combustion well. To this end, we observe that the recent comprehensive review by Glarborg et al. [23] on the NO_x chemistry in combustion of light hydrocarbons and the chemistry of nitrogen-containing species (HCN, NH_3, HNCO) provides a rational starting point for the current analysis. In particular, the various submodels of the nitrogen chemistry in the NO_x kinetic model proposed therein have been tested against a wide range of experimental conditions typically using small hydrocarbons as the fuel reactants. For larger hydrocarbons, the formation and consumption of fuel-derived radicals are more complex and their effects on NO_x formation remain not as well understood. For this reason, we measured NO_x concentrations in a series of premixed, stagnation flames of Jet A that span from fuel-lean to fuel-rich conditions and over a range of flame temperatures. To verify the applicability and accuracy of the HyChem foundational chemistry model for NO_x prediction, measurements were also made in methane and ethylene flames under similar conditions. Predictions of NO_x concentrations were then made using the HyChem Jet A (POSF10325) reaction model combined with the NO_x model of Glarborg et al. [23] and compared with the experimental data.

2. Experimental methodology

The premixed stretch-stabilized stagnation flame configuration used herein is similar to the setup deployed earlier to study soot formation in jet-fuel flames [24]. As shown in Fig. 1, the system comprises a burner with an aerodynamically shaped nozzle 1.43 cm in exit diameter, a stagnation surface/sampling probe assembly and a NO_x chemiluminescence analyzer. Jet A (POSF10325) is metered in the liquid form using a syringe pump (Harvard PHD2000) and injected into a vaporization chamber using a micro-orifice atomization nozzle. The chamber is entrained with a flow of N_2 at 483 K. The resulting vapor mixture of Jet A and N_2 is mixed with O_2 and the remaining N_2 before reaching the burner nozzle body. All gas lines are maintained at 483 K and the burner temperature is set at 513 K. Experiments are made also using methane and ethylene as fuels, in which case the unburned gas flow lines were unheated, except for a stoichiometric methane flame (see, Table 1), in which the lines were heated similarly to Jet A flames. A nitrogen sheath flow with the velocity that matches that of the unburned gas flow minimizes the flame edge effects [25]. The dis-

tance between the burner nozzle and stagnation plate, L, was held at 1.4 cm. The distance between the flame and stagnation surface/sampling probe, L_s, is varied by changes in the unburned gas velocity.

The temperature at the stagnation surface, T_s, was measured by a type-K thermocouple placed flush with the surface such that the bead is exposed to the sample gas at a radial distance of 1 cm from the centerline of the flame. The uncertainty of T_s is ± 15 K and this value is one standard deviation across all flames studied, similar to our previous study on Jet A flames performed with the same setup [24]. The temperature of the unburned gases, defined as T_u, was measured also with a type-K thermocouple inserted inside the burner nozzle with the tip 2 cm upstream of the nozzle exit to avoid disturbing the flame. Neither temperature measurement was corrected for radiation because they are too low for it to be important. The NO_x measurements were carried out over duration of 2 min for each flame, during which the unburned gas temperature varied < 5 K between the centerline and the wall of the burner body.

The flame standing distance L_s and flame thickness δ were determined experimentally by flame luminosity. A Canon Rebel T5i DSLR was used with a shutter speed of 1/100 s and field of view of 12 cm $\times$ 8 cm. The position was calibrated by imaging a ruler at the flame image plane to obtain the pixel per millimeter count in the flame image plane. To account for slight flame oscillations, 3 flame images were processed and averaged for each flame studied. The luminosity was determined as a function of axial and radial position and a Sobel edge detection algorithm in ImageJ was used to detect the edges of the blue flame zone, of which details can be found in Section S1 of the Supplementary Material. The flame position was measured to the center of the blue flame zone, and the flame thickness was measured at the centerline of the flame.

NO and NO_2 concentrations were measured at the stagnation surface along the center axis of the flame. The stagnation plate is water-cooled and also acts as a sampling probe. A micro-orifice (500 μm diameter, 125 μm wall thickness) is embedded within the stagnation plate. It draws the flame sample continuously. A NO_x analyzer with a chemiluminescence detector (CLD) (Eco Physics CLD 822 S h) is used to quantify NO, NO_2 and NO_x concentrations. The minimum detectable concentration of the instrument is 0.25 ppm.

Three or more series of flames were examined for each fuel tested. Each series has a given equivalence ratio but the unburned gas velocity was varied. For each series, three flames (*a*, *b* and *c*) were simulated; their flame parameters are listed in Table 1. Series *d*, *e* and *f* were designed to explore the effect of higher temperatures on NO_x production in Jet A flames and the influence of preheating the system in CH_4 flames. For the methane and Jet A flames, three equivalence ratios were tested to cover the variations of thermal and prompt NO_x. The flames are labeled by "fuel"-

Table 1

Experimental flame parameters and results.[a]

Flame	Unburned gas (mol%)			$T_u \pm 5$ (K)	$T_s \pm 15$ (K)	v_0 (cm/s)[b]	$L_s \pm \delta/2$ (cm)[b, c]	$T_{f,max}$ (K)[d]	NO_x (PPM)[e]
	Fuel	O_2	N_2						
CH_4-0.7-a	8.23	23.52	68.25	341	549	86.2	0.88±0.05	2082	33.0 ± 3.0
CH_4-0.7-b	8.06	23.02	68.92	332	534	88.0	0.81±0.05	2045	24.5 ± 1.8
CH_4-0.7-c	7.71	22.03	70.26	327	540	92.0	0.58±0.05	1972	16.4 ± 1.3
CH_4-1.0-a	8.98	17.97	73.05	335	548	79.0	0.80±0.04	2115	57.2 ± 4.0
CH_4-1.0-b	8.76	17.52	73.72	341	552	81.0	0.69±0.05	2066	44.9 ± 0.4
CH_4-1.0-c	8.35	16.70	74.95	340	561	85.0	0.52±0.05	1984	32.3 ± 1.9
CH_4-1.3-a	12.14	18.67	69.19	387	517	63.0	0.93±0.05	2100	85.2 ± 2.4
CH_4-1.3-b	11.59	17.82	70.59	386	515	66.0	0.62±0.05	2012	73.0 ± 1.2
CH_4-1.3-c	11.42	17.56	71.02	386	517	67.0	0.55±0.05	1985	70.0 ± 0.5
CH_4-1.0-d	8.59	17.19	74.22	496	521	82.6	0.84±0.06	2155	74.3 ± 14.1
CH_4-1.0-e	8.19	16.38	75.43	496	524	86.6	0.65±0.05	2072	53.3 ± 2.3
CH_4-1.0-f	7.83	15.65	76.52	496	523	90.7	0.50±0.05	1990	40.7 ± 2.3
C_2H_4-1.24-a	5.71	13.80	80.49	321	367	55.1	0.95±0.05	1871	52.1 ± 1.2
C_2H_4-1.24-b	5.51	13.32	81.17	329	390	57.1	0.65±0.03	1823	49.0 ± 2.1
C_2H_4-1.24-c	5.32	12.88	81.80	328	401	59.0	0.51±0.05	1766	44.6 ± 1.5
Jet A-0.7-a	0.75	17.98	81.27	496	465	53.5	1.01±0.07	1822	11.9 ± 0.6
Jet A-0.7-b	0.73	17.30	81.97	496	477	55.6	0.73±0.05	1767	9.6 ± 0.8
Jet A-0.7-c	0.70	16.70	82.60	496	498	57.6	0.53±0.05	1671	8.6 ± 0.2
Jet A-1.0-a	0.84	14.06	85.10	496	491	48.2	1.04±0.05	1884	37.7 ± 2.9
Jet A-1.0-b	0.80	13.52	85.68	496	492	50.1	0.77±0.06	1811	27.9 ± 0.4
Jet A-1.0-c	0.77	13.00	86.23	496	495	52.1	0.57±0.07	1703	16.7 ± 0.7
Jet A-1.3-a	1.01	13.03	85.96	496	400	43.2	0.70±0.09	1709	61.3 ± 0.2
Jet A-1.3-b	0.97	12.55	86.48	496	403	44.8	0.51±0.09	1643	52.2 ± 2.1
Jet A-1.3-c	0.96	12.37	86.67	496	404	45.5	0.49±0.09	1623	51.1 ± 2.3
Jet A-0.7-d	0.80	19.21	79.99	496	419	62.7	1.04±0.08	1902	19.4 ± 2.0
Jet A-0.7-e	0.77	18.52	80.71	496	441	65.0	0.78±0.06	1850	15.3 ± 4.0
Jet A-0.7-f	0.75	17.93	81.32	496	459	67.1	0.64±0.06	1781	8.9 ± 3.0
Jet A-1.0-d	0.88	14.92	84.20	496	442	57.0	0.99±0.07	1948	48.0 ± 3.3
Jet A-1.0-e	0.85	14.39	84.76	496	453	59.1	0.76±0.06	1875	35.2 ± 1.3
Jet A-1.0-f	0.83	14.04	85.13	496	458	60.6	0.62±0.06	1807	26.4 ± 1.3
Jet A-1.3-d	1.11	14.27	84.62	496	415	45.5	1.01±0.08	1813	78.3 ± 2.9
Jet A-1.3-e	1.07	13.76	85.17	496	420	47.2	0.79±0.07	1773	71.0 ± 1.6
Jet A-1.3-f	1.03	13.25	85.72	496	418	49.1	0.54±0.04	1728	57.3 ± 7.0

[a] The table lists flames that were both experimented and modeled. When available, NO_x measured for additional flames are shown in various figures. The complete data of all the flames examined is included in Table S1 of the Supplementary Material.

[b] STP conditions (298 K, 1 atm). Nozzle-to-stagnation surface separation is 1.4 cm.

[c] Flame position relative to the stagnation surface.

[d] Computed maximum flame temperature.

[e] NO_x concentration measured at the stagnation surface and its two-standard deviation.

"equivalence ratio"-"flame series." For example, CH_4-0.7-a refers to the methane flame with equivalence ratio of 0.7 and the lowest cold gas velocity; Jet A-1.3-c refers to the Jet A flame that has the highest cold gas velocity and equivalence ratio of 1.3 (see Table 1).

3. Computational approach

A modified OPPDIF code [26] is used here to compute the species profiles. Plug flow is assumed at the burner boundary, and non-slip boundary conditions are assumed at the stagnation surface. The net diffusive velocity at the stagnation surface is set to zero due to the balance of Fickian and thermal diffusion fluxes [27]. For the energy equation, the boundary conditions are given by the measured unburned gas temperature and the temperature measured at the stagnation surface. Numerical simulations are performed using multicomponent transport, thermal diffusion and with radiation corrections [28]. Heat release rates and transport properties were computed using the Chemkin suite of package [29, 30]. NO and NO_2 mole fractions were computed and the maximum NO_x ($NO + NO_2$) levels are used to compare with the experimental data for reasons to be discussed later.

The recent NO_x chemistry proposed by Glarborg et al. [23] is added to the HyChem Jet A model [2]. The HyChem foundational chemistry model is USC Mech II [31]. As the CH_x ($x = 1,2$) chemistry is critical to prompt NO formation, we tested the combined model against NO production in methane and ethylene flames. As will be discussed later, the comparison is satisfactory, and as

such no modification of the reaction kinetics was applied to either model. The combined HyChem-Glarborg (HG) model consists of 201 species and 1589 reactions. Model reduction has been conducted and is discussed in Section 5. The detailed, skeletal and reduced reaction models developed in this work are available in the Supplementary Material. Additionally, the models are also available on the HyChem webpage at https://web.stanford.edu/group/haiwanglab/HyChem/pages/download.html.

4. Results and discussions

4.1. Jet A stretched-stabilized flame structure

A numerical solution of a Jet A flame is shown in Fig. 2. The structure is typical of stretch-stabilized flames. The preheat zone of the flame is removed from the burner nozzle. The rise in temperature occurs where the local flow velocity approaches the stretched laminar flame speed of the unburned mixture. The variation in the unburned gas velocity corresponds to changes in the global strain rate, which in turn causes the flame standing distance and the reaction time to vary. The flame structure is similar across the range of the cold gas velocity used.

Caution was taken to ensure that the computed thermal mixing layer is comparable to that of the experimental flames. In particular, the computation used the plug flow boundary condition, whereas in the actual flames the flow boundary condition lies between the plug and potential flow limits. In this study, flames
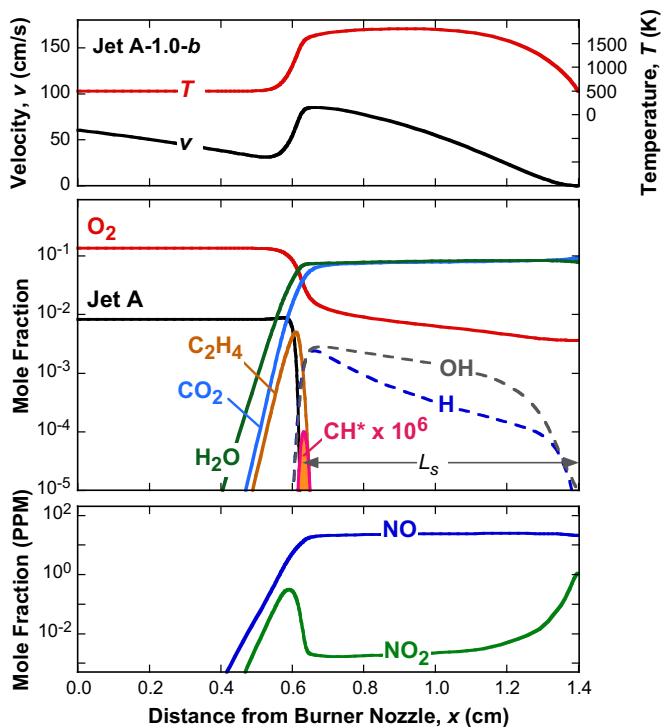
Fig. 2. Typical profiles of temperature and velocity (top panel), mole fractions of key flame species (middle panel), and NO and NO_2 (bottom panel), computed for the Jet A-1.0-*b* flame (see, Table 1).

were modeled by matching the observed standing distance, L_s, with the computed distance between the peak CH* position and the stagnation surface. This approach is similar to our previous work on stretch-stabilized ethylene flames [25]. For comparison, the L_s value computed for Jet A-1.0-*b* is 0.77 cm, whereas the measured value is 0.77±0.06 cm. Here, we tested two approaches to matching the flame standing distance. In both approaches, we assume the temperature inside the burner to stay relatively constant, thereby specifying the unburned gas temperature at the nozzle exit to be the value measured 2 cm upstream of the nozzle exit. The first approach specifies the cold-gas velocity v_0 as measured, while extending the computational domain towards the upstream, by between 0 and 2 cm, to match the experimentally measured L_s. The second approach is to fix the computational domain L at 1.4 cm, while decreasing the cold gas velocity v_0 to match the flame standing distance. A series of calculations applying the two approaches is performed for several Jet A flames, and the results are included in Fig. S3 of the Supplementary Material. Overall, the difference of computed NO_x concentration using the two approaches is quite small (within 9%). In essence, as long as the computed flame standing distance closely matches the experiment values, the chemical reaction residence time in the post flame zone is expected to be captured well. In the current work, we choose the first approach because of its relatively low computational cost.

In almost all the cases, the NO_2 concentration is substantially lower than the NO concentration, both in the flame and on the stagnation surface, as can be seen in Fig. 2. The NO concentration levels off in the post flame region. The rise of the NO_2 concentration toward the stagnation surface is due to conductive cooling of the gas as it is convected to it, leading the equilibrium shift to NO_2 in the fuel lean and stoichiometric mixtures. Because of the finite residence time (∼1 min) of the sample gas in the sample probe as it is carried to the NO_x analyzer, additional NO conversion to NO_2 may occur in the experiments, particularly for the fuel lean flames in which there is an excess of oxygen in the products. For this rea-
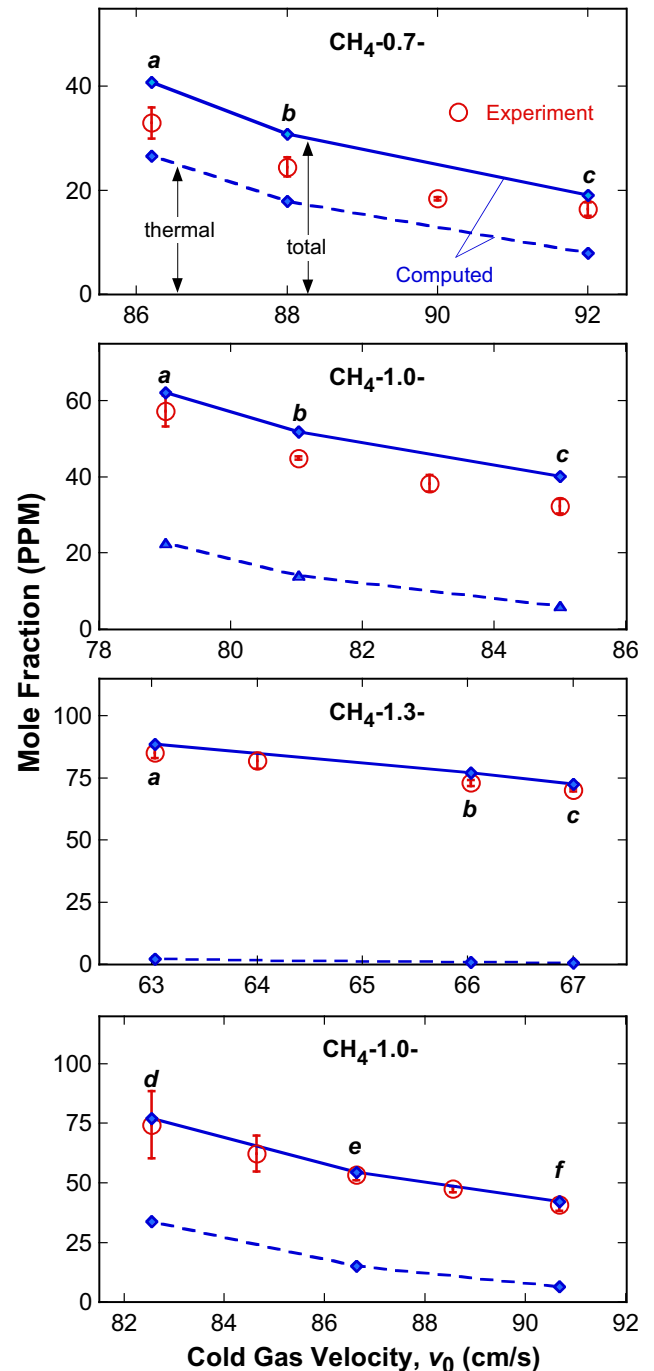

Fig. 3. Experimental (open symbols) and computed (filled symbols with lines drawn to guide the eyes) NO_x mole fractions versus the experimental cold gas velocity for the four series of methane flames. The flames are labeled as CH_4-ϕ-*x*, where ϕ is the equivalence ratio, and $x = a, b, c, d, e$ and f as indicated in Table 1. The error bars represent 2σ experimental data repeatability. The solid lines denote the total (thermal + prompt) NO_x computed; the dashed lines represents the NO_x concentrations computed using reactions involved in the thermal pathways only.

son, experiment-model comparisons are made between total NO_x measured versus the maximum of $NO + NO_2$ computed.

4.2. NO_x formation from methane and ethylene flames

For a typical Jet A fuel, methane (CH_4) and ethylene (C_2H_4) are considered to be the most dominant intermediate species during fuel thermal decomposition. NO_x formation from methane and

ethylene flames was thus studied first to assess the accuracy of the foundational fuel chemistry part of the HyChem model for NO_x prediction. Methane flames were examined at three equivalence ratios ($\phi = 0.7$, 1.0 and 1.3). The range of flame stoichiometries extends from the thermal NO dominated path to the predominantly the prompt NO path. Only one series of ethylene flame at $\phi = 1.24$ was studied mainly for testing the prompt NO chemistry.

The results for the methane flames are shown in Fig. 3. The experimental data are averaged over three runs for each case. The predicted NO_x concentration is the maximum sum of NO and NO_2 concentrations. Experimentally and computationally, the NO_x concentration in each series of the flame decreases with an increase in the experimental cold gas velocity. This is expected because the increase in the velocity increases the strain rate and decreases the distance from the flame to the stagnation surface and thus the reaction time. Furthermore, the reduced flame to stagnation surface distance causes more heat loss to the surface and hence leads to a reduced maximum flame temperature $T_{f,max}$ from flame a to c for each flame series (see, the second last column of Table 1).

The computed, total NO_x concentration is slightly higher than the experimental values at $\phi = 0.7$, and the agreement becomes better at $\phi = 1.0$. Overall, the modeled results agree well with the experimental data. As seen, the sources of NO_x are both thermal and prompt at $\phi = 0.7$ with the thermal NO accounting for between 40% to 66% of the total NO_x. The prompt NO is predominant at $\phi = 1.3$ and accounts for more than 97% of the total NO_x. Suffice it to note that in computing the contribution of thermal NO_x, we removed all N-species reactions except for the following reactions: $N + NO = N_2 + O$, $N + O_2 = NO + O$, and $N + OH = NO + H$, whereas the total NO_x was computed using the entire NO_x submodel.

As mentioned in Section 2, the Jet A flames require burner heating to prevent fuel condensation. To assess the sensitivity and effect of burner heating on NO_x formation and prediction, one additional series of methane flames were studied in which the burner and its gas lines are heated. The preheated unburned gas temperature at burner nozzle T_u is controlled to be identical to that of the Jet A flames. The result is shown in the bottom panel of Fig. 3. As seen, the predicted NO_x concentrations are in excellent agreement with the experimental values.

NO_x production was also measured and computed for a series of ethylene flames at $\phi = 1.24$. The results in Fig. 4 show again an excellent agreement between the experiment and model across the range of the cold gas velocity tested. It is seen that the total NO_x production is dominated by the prompt NO pathway. The thermal NO accounts for about 1% or less of the total NO_x production.

4.3. NO_x production in Jet A flames

Six series of Jet A flames were investigated at the equivalence ratios of 0.7, 1.0 and 1.3 with the d, e and f series having higher maximum flame temperatures than the a, b and c series, respectively (see, Table 1). The results are presented in Fig. 5. For reasons already discussed, the NO_x production is observed to decrease with an increase in the experimental cold gas velocity. The model predicts the same trend. To a large extent, the level of agreement between the experiment and model is similar to that of the methane flames. Unlike the methane flames, the computed NO_x production is systematically lower than experiment at $\phi = 1.3$ by 18% to 36%, while the comparison yields mostly satisfactory results at $\phi = 0.7$ and 1.0. A first inspection about this issue is that whether there is a noticeable amount of NO_x produced by the fuel-NO route that is not captured by the reaction model. Jet A (POSF10325) contains some heteroatoms as documented in the Supplementary Material of [24]. Experiments were carried out for a Jet A-O_2-Ar mixture under similar conditions, and the NO_x concentration is below the 0.25 ppm detection limit of the analyzer, indicating no appreciable
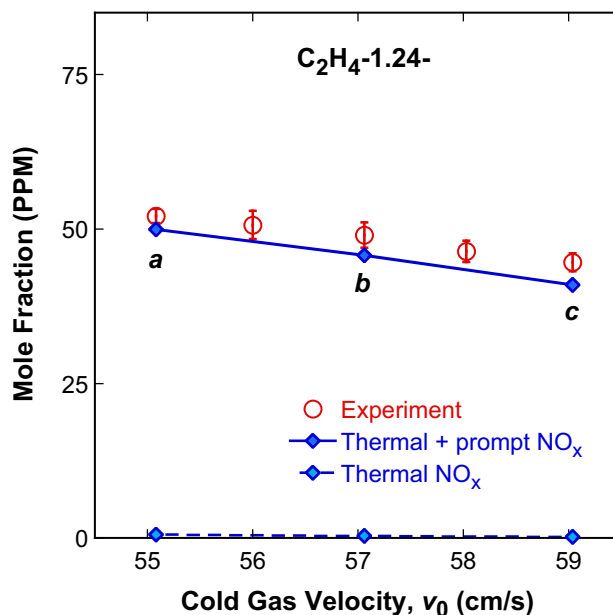

Fig. 4. Experimental (open symbols) and computed (filled symbols with lines drawn to guide the eyes) NO_x mole fractions versus the experimental cold gas velocity for the ethylene flames. The flames are labeled as C_2H_4-ϕ-x, where ϕ ($\phi = 1.24$) is the equivalence ratio, and $x = a$, b, and c as indicated in Table 1. The error bars represent 2σ experimental data repeatability. The solid line denotes the total NO_x computed; the dashed line represents the NO_x concentrations computed using reactions involved in the thermal pathways only.

NO from the fuel. To investigate the source of discrepancies, we will present and report sensitivity tests in the next two sections.

As shown in Fig. 5, the thermal NO route accounts for between 9% to 44% of the total NO_x production at $\phi = 0.7$, and 3% to 23% at $\phi = 1.0$. The prompt NO production is extremely dominant at $\phi = 1.3$. The relative importance of the thermal NO is generally lower in the Jet A flames than in the CH_4 flames under comparable conditions. The primary reason is the somewhat lower maximum flame temperatures in Jet A flames than in the CH_4 flames (see, Table 1).

4.4. Sensitivity with respect to flame simulation uncertainties

As mentioned in Section 2, the flame standing distance L_s, the unburned gas temperature at burner nozzle T_u, and the stagnation surface T_s are measured with uncertainties. As described in Table 1, the uncertainties of the measured L_s vary from ± 0.04 to ± 0.09 cm (Table 1). Here, we perform sensitivity analyses of NO_x production for Jet A-1.0-a, b, and c flames with respect to their L_s uncertainties. The results suggest that there is very little to no sensitivities to the uncertainties in L_s (see, Fig. S4 of the Supplementary Material). Specifically, the largest sensitivity is observed for the Jet A-1.0-c flame, which has the smallest L_s value but the largest absolute uncertainty among the three flames tested ($L_s = 0.57 \pm 0.07$ cm). Figure 6 shows the temperature, centerline velocity, and NO mole fraction profiles computed for the Jet A-1.0-c flame considering the experimental uncertainties in L_s. As seen, the ± 0.07 cm variation in flame standing distance leads to the predicted NO mole fractions to vary within 1.1 ppm. We consider this level of uncertainty to be the maximum of the simulation errors that could result from experimental flame position uncertainty among all flames studied. Sensitivity analyses are also conducted for the same Jet A flames with respect to ± 5 K and ± 15 K uncertainties of T_u and T_s. Again, the variations of predicted NO_x mole fractions are well within 1 ppm or <5% of the nominally predicted
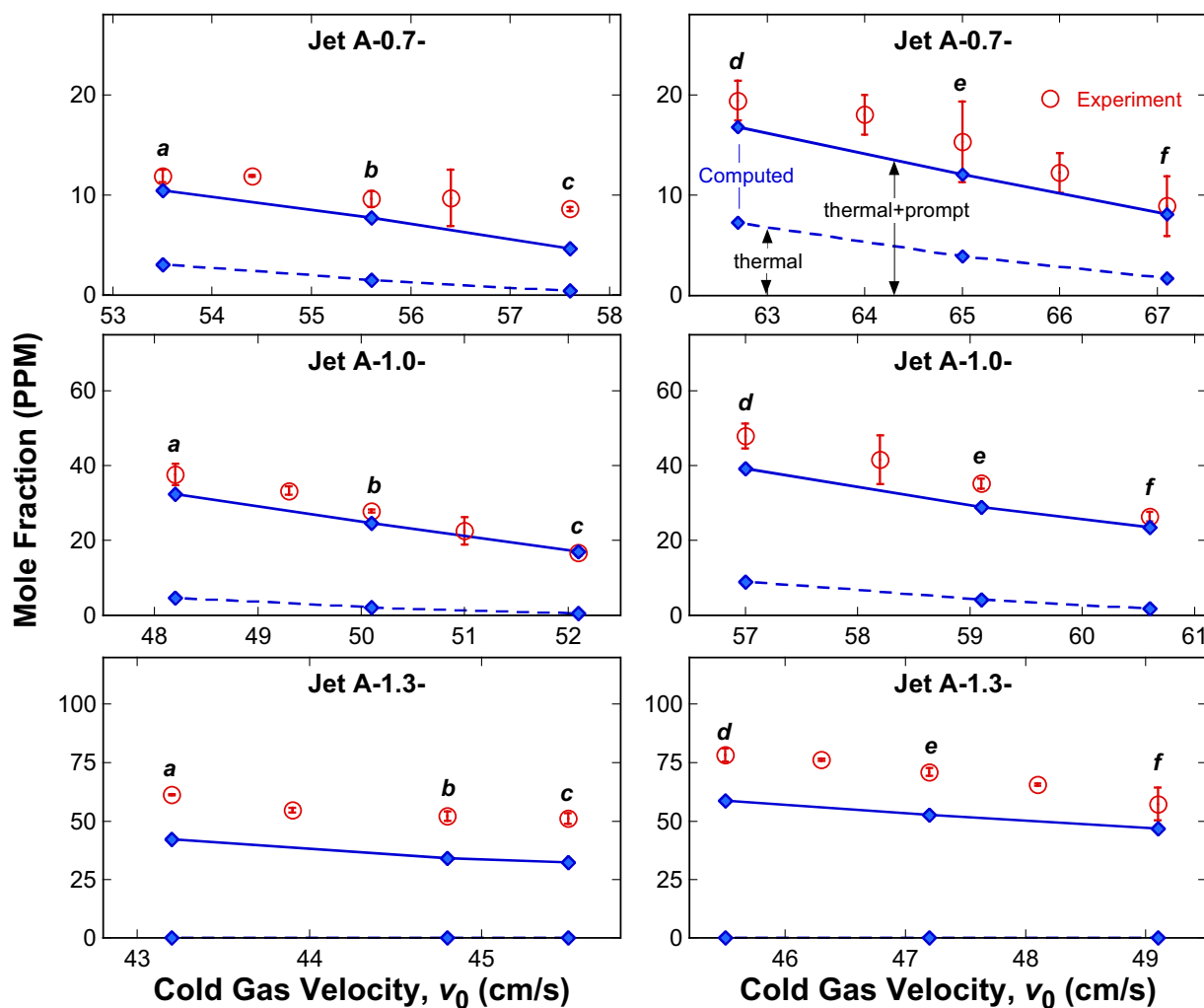
Fig. 5. Experimental (open symbols) and computed (filled symbols with lines drawn to guide the eyes) NO_x mole fractions versus the experimental cold gas velocity for the Jet A flames. The flames are labeled as Jet A-ϕ-x, where ϕ is the equivalence ratio, and $x = a$, b, c, d, e and f as indicated in Table 1. The error bars represent 2σ experimental data repeatability. The solid lines denote the total NO_x computed; the dashed lines represent the NO_x concentrations computed using reactions involved in the thermal pathways only.

values (see, Figs. S5 and S6 of the Supplementary Material). In conclusion, the experimental uncertainties in L_s, T_u and T_s lead to little or no impact on the results of the numerical simulation.

4.5. Sensitivity with respect to kinetic rate constants

Brute force sensitivity analyses of NO_x production in Jet A-0.7-e, Jet A-1.0-e, and Jet A-1.3-e flames are obtained in order to evaluate the influence of reaction pathways on NO_x formation and to reveal possible causes for the observed experiment-model discrepancies in NO_x concentrations. The results are presented as ranked sensitivity spectra in Fig. 7. No fuel-specific reaction in the HyChem model plays a role in the prediction of NO_x formation, as expected. At $\phi = 0.7$, NO_x production is sensitive to thermal NO reaction (e.g., $N + NO = N_2 + O$), prompt NO reactions (e.g., $CH + N_2 = H + NCN$), and reactions related to the CH chemistry which initiates the prompt NO pathway (e.g., $CH + H_2 = CH_2 + H$, and $CH + O_2 = HCO + O$). Moreover, the production of NO_x is also sensitive to the reactions related to N_2O, which is classified as one source of prompt NO pathway as well [17]. For the stoichiometric flame, the thermal NO pathway becomes less important, as the sensitivity coefficient of $N + NO = N_2 + O$ drops by a factor of 3; the prompt NO reactions becomes more significant in impacting NO production. At $\phi = 1.3$, the prompt NO route dominates the NO_x

production; the importance of NCN reactions ($NCN + O = CN + NO$ and $NCN + H = HCN + N$) becomes more significant. The sensitivities to the CH reactions are likewise prominent. No re-burn reactions appear to impact NO formation, suggesting their negligible importance under the flame conditions tested.

Whether the experiment-model discrepancy observed at $\phi = 1.3$ is an indication of one or more missing pathways in prompt NO formation remains to be an open question. To date, there have been only a limited number of investigations of prompt NO chemistry for fuels other than methane. The few studies available for NO production from flames of larger hydrocarbon fuels have shown NO formation to be more poorly predicted than in CH_4 flames. For example, in the work of Sutton et al. [32], NO was found to be underpredicted for the C_2–C_4 fuels under fuel rich and stoichiometric conditions, and for fuel rich flames, the discrepancy increases as the fuel size increases. Similar disagreement was found in Watson et al. [33], again for fuel-rich premixed flames of C_1–C_4 alkanes and alcohols. It is has been suggested that the C_3H_x radicals, including C_3H_3, C_3H_2, and C_3H, could become important in interacting with the nitrogen chemistry [23]. The propargyl radical (C_3H_3) is included in the foundational fuel chemistry part of the HyChem model. The mole fraction level of (C_3H_3) can be one order of magnitude higher than that of CH in the Jet A flames (e.g. $\sim$10 PPM C_3H_3 vs. 1 PPM CH in Jet A-1.3-b). On comparison, the peak
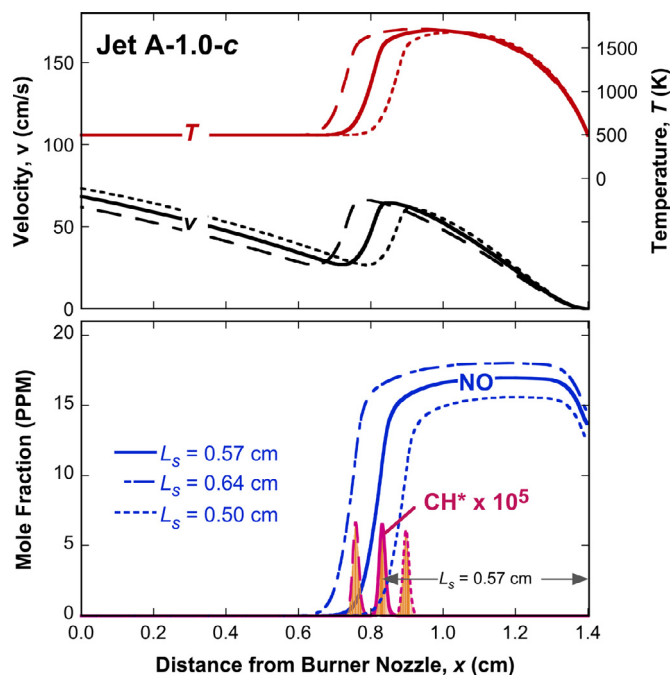
Fig. 6. Sensitivities of predicted temperature, centerline velocity and NO profiles with respect to flame standing distance L_s.

concentrations of C_3H_3 and CH in the CH_4 flame series are both ~1 PPM. The higher C_3H_3 production in the Jet A flame is primarily due to the reactions of propene (C_3H_6), a major pyrolysis product of Jet A [2]. Additionally, the rate constant uncertainties in the CH reactions and the prompt NO reactions could be another factor in explaining the discrepancies observed in predicted NO_x concentrations of the fuel-rich Jet A flames. Future work will need to assess the interaction of C_3H_x radical with nitrogen chemistry.

5. Model reduction

The combined reaction model is systematically reduced for computationally efficient CFD simulations. The reduction is performed based on the sampled reaction states sampled from auto-ignition and perfectly stirred reactors (PSR) over pressure of 0.5–60 atm, equivalence ratio of 0.5–1.5, inlet temperature of 300 K for PSR, and initial temperature of 1000–1600 K for auto-ignition. Skeletal reduction is performed using the method of directed relation graph (DRG) [34] and DRG-aided sensitivity analysis (DRGASA) [35]. Time-scale reduction is then applied using the linearized quasi-steady-state approximations (LQSSA) [36].

In DRG, hydrogen atom (H) and NO are selected as the starting species with a worst-case error tolerance of 0.3, resulting in a 129-species skeletal model. DRGASA is then applied with ignition delay, residence time and NO concentrations at selected temperatures on the S-curve of PSR as target parameters.

Figure 8 shows the reduction curve in DRGASA. It was found that while the number of species rapidly decreases for worst-case errors less than 0.2, the reduction error significantly increases if a few species are further eliminated. Thus, a 71-species skeletal model is obtained by choosing the error threshold of 0.2. Timescale based reduction is then performed on the skeletal model using the same sampled reaction states in the skeletal reduction, and twenty species are identified as global quasi-steady state (QSS) species using a criterion based on computational singular perturbation (CSP) [36], resulting in a 51-species reduced model. The QSS species are hidden from the transport equations and their concentrations can be analytically solved using internal algebraic equations [37].
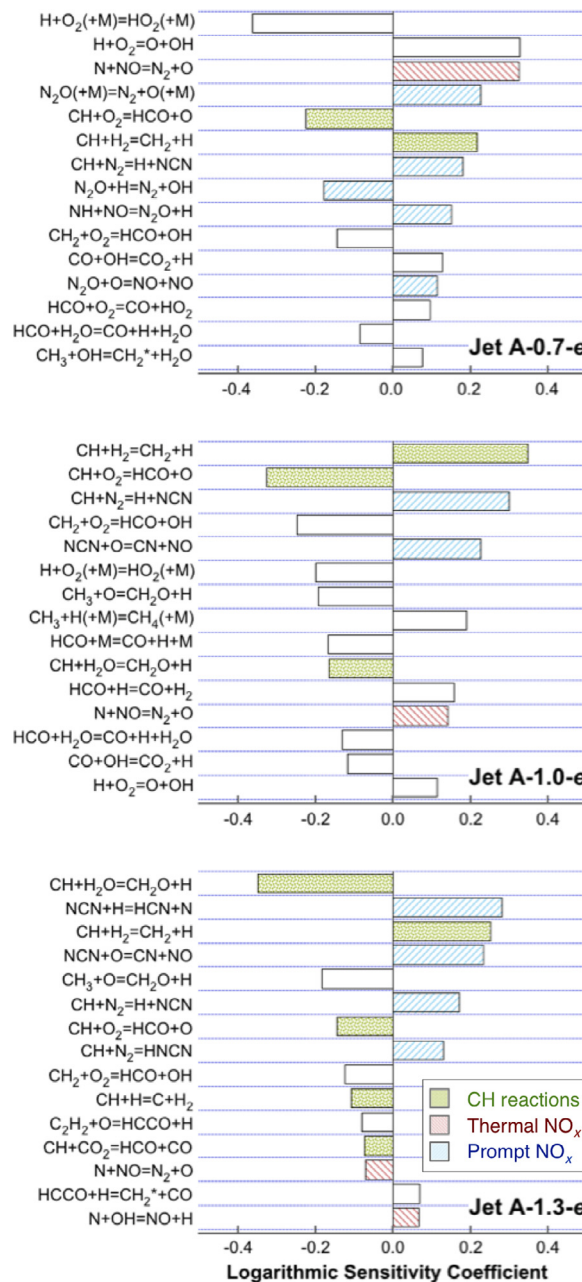

Fig. 7. Ranked sensitivity spectra of NO_x production for the Jet A-0.7-*e* (top panel), Jet A-1.0-*e* (middle panel), and Jet A-1.3-*e* (bottom panel) flames.
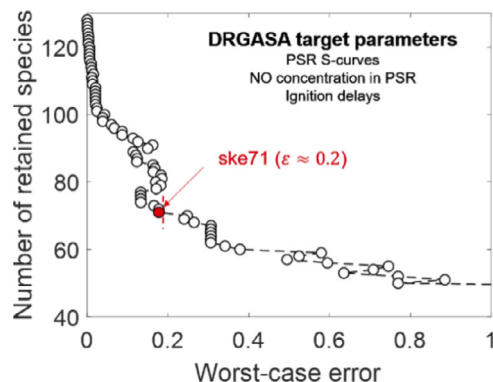

Fig. 8. Number of retained species as a function of the user-specified relative error tolerance in DRGASA.
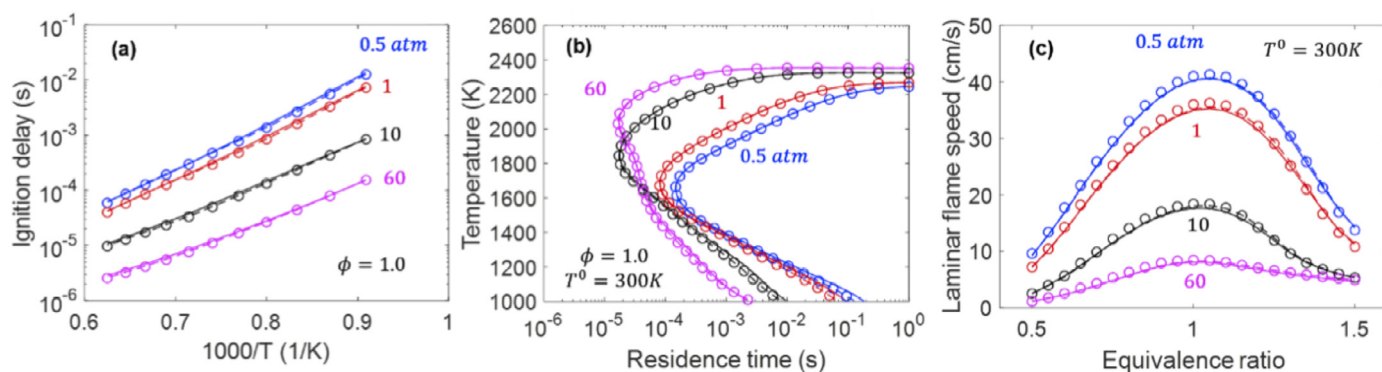
Fig. 9. Validation of the skeletal and reduced models for (a) ignition delay, (b) PSR extinction, and (c) laminar flame speed with free stream temperature of 300 K, for Jet A (POSF10325)/air. Detailed: solid lines, skeletal: dotted lines, reduced: symbols.
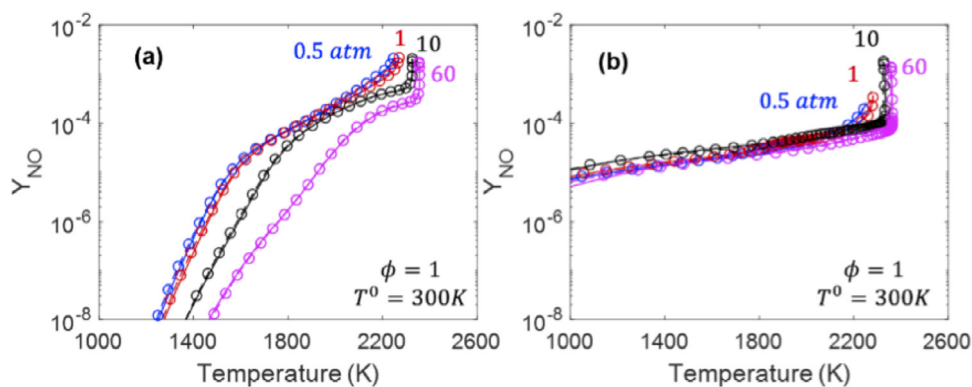

Fig. 10. NO concentration predicted by using the detailed, skeletal and reduced models, respectively, for (a) PSR and (b) premixed flames of stoichiometric Jet A (POSF10325)/air with inlet temperature of 300 K. Detailed: solid lines, skeletal: dotted lines, reduced: symbols.

Figure 9 shows the selected validation results for the skeletal and reduced models against the detailed model for ignition delay, PSR extinction, and laminar flame speed with NO concentrations shown in Fig. 10 for PSR and premixed flames. The worst-case error is approximately 13% for ignition delay, 5% for PSR extinction residence time, and less than 2 cm/s for flame speed. Similar agreements are observed for lean and rich mixtures ($\phi = 0.5$–1.5) for ignition delay and PSR extinction.

Test results for the skeletal and reduced models for NO_x prediction under the current experimental conditions are shown in Fig. S7 of the Supplementary Material. As seen, the results calculated by skeletal and reduced model are in good agreement with the nominal predictions with the errors within 15%, which is below the 20% threshold of DRGASA. The errors are primarily caused by the predictions of the maximum flame temperature. For example, in the worst case (Jet A-0.7-*b*), the maximum flame temperature is predicted as 1767 K, 1752 K, and 1753 K by the nominal, skeletal, and reduced models, respectively. Whereas at the best-case error condition (Jet A-1.3-*b*), the maximum flame temperature is predicted as 1643, 1647, and 1645 K by the nominal, skeletal, and reduced models, respectively. Additional tests for the maximum flame temperature for premixed and non-premixed counterflow flames are presented in Fig. S8 of the Supplementary Material.

6. Conclusions

NO_x formation was studied in stretch-stabilized premixed flames of methane, ethylene, and a typical Jet A (POSF10325) over a range of mixture compositions and operating conditions. NO_x production from those flames was simulated using a HyChem

model [2] combined with the NO_x chemistry of Glarborg et al. [23]. The accuracy of the combined model was first assessed for methane and ethylene flames. Overall, the model gives good agreement with the experimental data, thus supporting the validity of the experimental set up, the simulation method, and the combined HyChem-NO_x reaction model. Subsequently, the simulated NO_x concentrations were compared with experimental data from the Jet A flames. The results show that the combined model captures the NO_x production well especially for the fuel-lean and stoichiometric flames. Some discrepancies were found for the Jet A flames at the equivalence ratio of 1.3, in which the prompt NO route is dominant, with the model under-predicting the experimental data to an extent. Sensitivity analysis on the flame boundary conditions shows that the uncertainties in the flame measurement have little effect on the model prediction. Sensitivity analyses of reaction pathways along with the comparison of NO_x production from fuel-lean to rich Jet A flames support the notion that minor prompt NO pathways involving C_3 or other larger hydrocarbon radicals deserve some attention and study in the future.

Declaration of Competing Interest

The authors declare that they have no known competing financial interests or personal relationships that could have appeared to influence the work reported in this paper.

Acknowledgments

Supplementary materials

Supplementary material associated with this article can be found, in the online version, at doi:10.1016/j.combustflame.2019.10.038.

References

[1] H. Wang, R. Xu, K. Wang, C.T. Bowman, R.K. Hanson, D.F. Davidson, K. Brezinsky, F.N. Egolfopoulos, A physics-based approach to modeling real-fuel combustion chemistry – I. Evidence from experiments, and thermodynamic, chemical kinetic and statistical considerations, Combust. Flame 193 (2018) 502–519.

[2] R. Xu, K. Wang, S. Banerjee, J. Shao, T. Parise, Y. Zhu, S. Wang, A. Movaghar, D.J. Lee, R. Zhao, X. Han, Y. Gao, T. Lu, K. Brezinsky, F.N. Egolfopoulos, D.F. Davidson, R.K. Hanson, C.T. Bowman, H. Wang, A physics-based approach to modeling real-fuel combustion chemistry – II. Reaction kinetic models of jet and rocket fuels, Combust. Flame 193 (2018) 520–537.

[3] K. Wang, R. Xu, T. Parise, J. Shao, A. Movaghar, D.J. Lee, J.-W. Park, Y. Gao, T. Lu, F.N. Egolfopoulos, D.F. Davidson, R.K. Hanson, C.T. Bowman, H. Wang, A physics-based approach to modeling real-fuel combustion chemistry – IV. Hychem modeling of combustion kinetics of a bio-derived jet fuel and its blends with a conventional Jet A, Combust. Flame 198 (2018) 477–489.

[4] R. Xu, H. Wang, Principle of large component number in multicomponent fuel combustion – a Monte Carlo study, Proc. Combust. Inst. 37 (2019) 613–620.

[5] Y. Tao, R. Xu, K. Wang, J. Shao, S.E. Johnson, A. Movaghar, X. Han, J.-W. Park, T. Lu, K. Brezinsky, F.N. Egolfopoulos, D.F. Davidson, R.K. Hanson, C.T. Bowman, H. Wang, A. Physics-based approach to modeling real-fuel combustion chemistry – III. Reaction kinetic model of JP10, Combust. Flame 198 (2018) 466–476.

[6] L. Esclapez, P.C. Ma, E. Mayhew, R. Xu, S. Stouffer, T. Lee, H. Wang, M. Ihme, Fuel effects on lean blow-out in a realistic gas turbine combustor, Combust. Flame 181 (2017) 82–99.

[7] A. Felden, L. Esclapez, H.Wang Riber, B. Cuenot, Including real fuel chemistry in large-eddy simulations, Combust. Flame 193 (2018) 397–416.

[8] J.M. Foale, A. Giusti, E. Mastorakos, Numerical investigation of lean blow-out of kerosene spray flames with detailed chemical models, 2019 AIAA SciTech Forum, San Diego, CA (2019) AIAA Paper 2019-2239.

[9] V.R. Hasti, P. Kundu, G. Kumar, S.A. Drennan, S. Som, J.P. Gore, A numerical study of flame characteristics during lean blow-out in a gas turbine combustor, 2018 Joint Propulsion Conference, Cincinnati, OH, (2018) AIAA Paper 2018-4955.

[10] A. Panchal, R. Ranjan, S. Menon, Effect of chemistry modeling on flame stabilization of a swirl spray combustor, 2018 Joint Propulsion Conference, Cincinnati, OH, (2018) AIAA Paper 2018-4684.

[11] Y. Tang, M. Hassanaly, V. Raman, B. Sforzo, J.M. Seitzman, Numerical simulation of forced ignition of Jet-fuel/air using large eddy simulation (LES) and a tabulation-based ignition, 2019 AIAA ScTech Forum, San Diego, CA, (2019) AIAA Paper 2019-2242.

[12] C.T. Wey, Fuel sensitivity of lean blowout in a RQL gas turbine combustor, 2019 AIAA Propulsion and Energy Forum, Indianapolis, IN, (2019) AIAA Paper 2019-4035.

[13] R.F. Kulakhmetov, T.L. Pourpoint, Numerical investigation of bulk velocity and pressure on near wall chemistry in fuel rich RP-2/GOX combustion, 2019 AIAA Propulsion and Energy Forum, Indianapolis, IN, (2019) AIAA Paper 2019-3940.

[14] M.F. Yost, Y. Choi, E.W. Lerner, J.F. Driscoll, Performance of a generic X-51 waverider – Thrust, drag, and trim computed using the MASIV reduced order model, 2019 AIAA Propulsion and Energy Forum, Indianapolis, IN, (2019) AIAA Paper 2019-3841.

[15] M. Colket, J. Heyne, M. Rumizen, M. Gupta, T. Edwards, W.M. Roquemore, G. Andac, R. Boehm, J. Lovett, R. Williams, J. Condevaux, D. Turner, N. Rizk, J. Tishkoff, C. Li, J. Moder, D. Friend, V. Sankaran, Overview of the national jet fuels combustion program, AIAA J. 55 (2017) 1087–1104.

[16] J.A. Miller, C.T. Bowman, Mechanism and modeling of nitrogen chemistry in combustion, Prog. Energy Combust. Sci. 15 (1989) 287–338.

[17] C.T. Bowman, Control of combustion-generated nitrogen oxide emissions: technology driven by regulation, Symp. (Int.) Combust 24 (1992) 859–878.

[18] S. Hill, L.D. Smoot, Modeling of nitrogen oxides formation and destruction in combustion systems, Prog. Energy Combust. Sci 26 (2000) 417–458.

[19] Y.B. Zeldovich, The oxidation of nitrogen in combustion and explosions, Acta Physicochim. URSS 21 (1946) 577–628.

[20] C.P. Fenimore, Formation of nitric oxide in premixed hydrocarbon flames, Symp. (Int.) Combust 13 (1971) 373–380.

[21] P.C. Malte, D. Pratt, The role of energy-releasing kinetics in NO_x formation: fuel-lean, jet-stirred CO-air combustion, Combust. Sci. Technol. 9 (1974) 221–231.

[22] J.W. Bozzelli, A.M. Dean, O+NNH: A possible new route for NO_x formation in flames, Int. J. Chem. Kinet. 27 (1995) 1097–1109.

[23] P. Glarborg, J.A. Miller, B. Ruscic, S.J. Klippenstein, Modeling nitrogen chemistry in combustion, Prog. Energy Combust. Sci. 67 (2018) 31–68.

[24] C. Saggese, A.V. Singh, X. Xue, C. Chu, M.R. Kholghy, T. Zhang, J. Camacho, J. Giaccai, J.H. Miller, M.J. Thomson, C.-J. Sung, H. Wang, The distillation curve and sooting propensity of a typical jet fuel, Fuel 235 (2019) 350–362.

[25] J. Camacho, A.V. Singh, W. Wang, R. Shan, E.K. Yapp, D. Chen, M. Kraft, H. Wang, Soot particle size distributions in premixed stretch-stabilized flat ethylene–oxygen–argon flames, Proc. Combust. Inst. 36 (2017) 1001–1009.

[26] A.E. Lutz, R.J. Kee, J.F. Grcar, F.M. Rupley, OPPDIF: A Fortran program for computing opposed-flow diffusion flames, Report No. SAND-96-8243, Sandia National Laboratories, Livermore, CA, 1997.

[27] A.D. Abid, J. Camacho, D.A. Sheen, H. Wang, Quantitative measurement of soot particle size distribution in premixed flames–the burner-stabilized stagnation flame approach, Combust. Flame 156 (2009) 1862–1870.

[28] F.N. Egolfopoulos, Geometric and radiation effects on steady and unsteady strained laminar flames, Symp. (Int.) Combust 25 (1994) 1375–1381.

[29] R.J. Kee, J.A. Miller, T.H. Jefferson, 1980 Chemkin: A general-purpose, problem-independent, transportable, FORTRAN chemical kinetics code package, Report NO. SAND-80-8003, Sandia National Laboratories, 1980.

[30] R.J. Kee, G. Dixon-Lewis, J. Warnatz, M.E. Coltrin, J.A. Miller, A Fortran computer code package for the evaluation of gas-phase multicomponent transport properties, Report NO. SAND-86-8246, Sandia National Laboratories, Albuquerque, NM, 1986., 1986.

[31] H. Wang, X. You, A.V. Joshi, S.G. Davis, A. Laskin, F. Egolfopoulos, C.K. Law, USC Mech Version II. High-temperature combustion reaction model of $H_2/CO/C_1$-C_4 compounds. http://ignis.usc.edu/Mechanisms/USC-Mech%20II/USC_Mech%20II.htm, 2007.

[32] J.A. Sutton, B.A. Williams, J.W. Fleming, Investigation of NCN and prompt-NO formation in low-pressure C_1–C_4 alkane flames, Combust. Flame 159 (2012) 562–576.

[33] G.M.G. Watson, P. Versailles, J.M. Bergthorson, NO formation in rich premixed flames of C_1–C_4 alkanes and alcohols, Proc. Combust. Inst. 36 (2017) 627–635.

[34] T. Lu, C.K. Law, A directed relation graph method for mechanism reduction, Proc. Combust. Inst. 30 (2005) 1333–1341.

[35] X. Zheng, T. Lu, C. Law, Experimental counterflow ignition temperatures and reaction mechanisms of 1, 3-butadiene, Proc. Combust. Inst. 31 (2007) 367–375.

[36] T. Lu, C.K. Law, A criterion based on computational singular perturbation for the identification of quasi steady state species: a reduced mechanism for methane oxidation with NO chemistry, Combust. Flame 154 (2008) 761–774.

[37] T. Lu, C.K. Law, Systematic approach to obtain analytic solutions of quasi steady state species in reduced mechanisms, J. Phys. Chem. A 110 (2006) 13202–13208.